Evidence of disorder in cubic zirconium tungstate from the temperature dependence of Raman spectra

2007 J. Phys.: Condens. Matter 19 226210

(http://iopscience.iop.org/0953-8984/19/22/226210)

IOP PUBLISHING JOURNAL OF PHYSICS: CONDENSED MATTER

J. Phys.: Condens. Matter **19** (2007) 226210 (15pp) doi:10.1088/0953-8984/19/22/226210

Evidence of disorder in cubic zirconium tungstate from the temperature dependence of Raman spectra

Akhilesh K Arora, T R Ravindran and Sharat Chandra

Materials Science Division, Indira Gandhi Centre for Atomic Research, Kalpakkam 603102 TN, India

E-mail: trr@igcar.gov.in

Received 16 October 2006, in final form 17 April 2007
Published 8 May 2007
Online at stacks.iop.org/JPhysCM/19/226210

Abstract

The cubic phase of zirconium tungstate exhibits a larger number of vibrational Raman modes in the frequency region of the symmetric stretching mode of tungstate ions than permitted by group-theoretical analysis for a perfectly ordered lattice. This suggests the existence of disorder in the tungstate sublattice. The additional modes are identified and assigned on the basis of their relative intensities and temperature dependences of line-widths. Using a real-space model for misoriented tetrahedral ions, the occurrence of four disorder modes is explained. From the evolution of the intensities of different components of the symmetric stretching mode as a function of temperature, the disorder is found to be largely static (frozen-in) in nature. As each tungstate ion carries a net dipole moment, randomly misoriented tetrahedral units can result in a dipole glass, explaining a recently reported glass-like behaviour of thermal conductivity. The proposed disordered configurations of tungstate ions are indeed found to be energetically stable from first-principles simulation studies.

1. Introduction

The discovery of large isotropic negative thermal expansion (NTE) over a wide range of temperature in zirconium tungstate $Zr(WO_4)_2$ [1] has generated a great deal of interest in this material [2–6] and related network structures [7–10]. Cubic zirconium tungstate (α-phase) belongs to the space group $P2_13$ (T^4) with four formula units per unit cell. The Zr atoms occupy fcc sites while eight tungstate tetrahedral ions are located at C_3 sites. As each zirconium atom has six oxygen neighbours, the structure could be viewed as a network of corner-sharing ZrO_6 octahedra and WO_4 tetrahedra [1]. Only three of the four oxygens of the WO_4 tetrahedra are shared with the neighbouring Zr ions, while the fourth oxygen, also known as the 'terminal oxygen', is bonded only to W and has significantly shorter W–O bond length compared to the other three W–O bonds. The shorter bond for the terminal O is attributed to the fact that the

negative charge of this atom is not shared with another cation. There are two distinct sets of four tungsten atoms labelled as W1 and W2 [1]. The tetrahedron around W1 is constituted by O4 (terminal) and three O1 oxygen atoms. On the other hand, O3 (terminal) and three O2 oxygen atoms form the other tetrahedron. The bond lengths and bond angles in the two tetrahedra are also different. Recent Raman spectroscopic studies [11] have revealed that only the internal modes of WO_4 tetrahedra [12] exist, while those corresponding to ZrO_6 octahedra are not found. This implied that in this compound WO_4 is a more strongly bound unit compared to ZrO_6 octahedra, leading to an alternate perception of the unit cell [11], where ZrO_6 is not treated as a rigid unit (e.g., as shown in figure 1 of [11]). Subsequent temperature-dependent x-ray absorption fine-structure (XAFS) studies have confirmed the flexibility of ZrO_6 units [3] and showed that the transverse vibrations of O in W–O–Zr linkage are not the primary mechanism of NTE in this material. A correlated translation–rotation motion of WO_4 along $\langle 111 \rangle$ axes has been argued to be the cause of contraction [6].

Zirconium tungstate is reported to undergo an order–disorder transition at 428 K [1, 13] at ambient pressure. At ambient temperature it exhibits an irreversible transition to an orthorhombic phase at 0.3 GPa [14] and amorphization at 2.2 GPa [2]. The high-temperature disordered phase involves flipping of both WO_4 tetrahedra along the C_3 axis, i.e., the tungsten-terminal oxygen bonds in both the WO_4 ions are either parallel or antiparallel to the C_3 axis with equal probability [1], and the space group changes to $Pa\bar{3}$. Many compounds that contain molecular ions such as sulfate, molybdate, and ammonium are often found to exhibit orientational disorder of these tetrahedral units [15–18]. If the disorder is among discrete/distinct orientations, one finds a larger number of internal vibrational modes of the polyatomic ion than predicted by group theory [17]. Furthermore, the disorder could be either static [17], or dynamic [16], or both [19]. On the other hand, a continuum of disordered states would make the ion a free rotator, resulting in the broadening of the characteristic internal vibrations of the tetrahedral ion [20, 21]. Existence of discrete orientational disorder has also been found to result in pressure-induced amorphization (PIA) in several compounds such as $LiKSO_4$ [17], potash alum [18] and scandium molybdate [15]. Interestingly, zirconium tungstate also undergoes PIA at a rather moderate pressure of 2.2 GPa. This raises the question whether this compound also has orientational disorder of tungstate ions. In this context it is important to point out that the temperature dependence of thermal conductivity of $Zr(WO_4)_2$ has been recently reported to be glass-like, which is not well understood [22]. In this paper we reexamine the temperature dependence of Raman spectra of internal modes of tungstate ions from the point of view of a possible tungstate ion disorder. A real-space model of misoriented WO_4 ions is presented to explain the occurrence of additional modes due to disorder. The stability of the proposed misorientations is also examined from first-principles density-functional calculations. The dipole moment associated with each of the WO_4 ions is calculated and the possibility of randomly misoriented dipoles leading to a dipole-glass state is discussed.

2. Experimental details

Polycrystalline powder and single-crystal samples of $Zr(WO_4)_2$ were used in the present study. Low-temperature Raman measurements from 20 to 300 K at 20 K intervals were carried out using an APD closed-cycle refrigerator. The temperature was controlled by a Lakeshore Model 330 autotuning temperature controller employing separate silicon diode thermometers for control and sample temperature measurement. Raman spectra were recorded in the backscattering geometry using the 488 nm line of an argon-ion laser. Scattered light from the sample was analysed by a SPEX double monochromator, and detected with a cooled

Table 1. Correlation table for the vibrational modes of tetrahedral tungstate ion in zirconium tungstate.

Free ion (T_d)	Site (C_3)	Crystal ($P2_13$: T^4)
$A(\nu_1)$	A	A
$E(\nu_2)$		E
F_1	E	F
$F_2(\nu_3, \nu_4)$		

photomultiplier tube operated in the photon-counting mode. Scanning of the spectra and data acquisition were carried out using a home-built microprocessor-based data acquisition cum control system. Subsequent to the completion of a scan, data were transferred to a personal computer for further analysis. Polarized Raman measurements were performed on thin crystallites of about 2 mm^2 lateral dimensions. The calculated depolarization ratio was corrected for the response of the monochromator to different polarizations.

3. Simulation details

In order to confirm whether the proposed misoriented configurations are energetically stable or not, we carried out density-functional calculations using the SIESTA code [23]. The fully relativistic Perdew–Burke–Ernzerhof generalized gradient approximation for exchange and correlation was used with partial core-correction for all atoms, along with a total of 64 ($4\times4\times4$) k-points in a Monkhorst–Pack grid. The energy cutoff was 200 Ryd, and a double zeta plus polarization (DZP) basis set was used. Standard norm-conserving, Troullier–Martins TM2 pseudopotentials were employed. The starting values of all the other parameters were kept the same during all the calculations. The computations were performed in a 16-node Linux cluster.

4. Results and discussion

According to the group-theoretical analysis of normal modes of zirconium tungstate presented earlier [11], one can classify these modes into acoustic, lattice and external and internal modes of tungstate tetrahedral ions. These groups of modes appear in different ranges of frequencies. From the knowledge of frequencies of a free tungstate ion [24] and those in other crystals [12, 25], one can assign the frequency ranges 250–320 cm^{-1} to the symmetric bending mode ν_2(E), 320–470 cm^{-1} to the antisymmetric bending mode $\nu_4(F_2)$, 620–890 cm^{-1} to the antisymmetric stretching mode $\nu_3(F_2)$ and 890–1050 cm^{-1} to the symmetric stretching mode ν_1(A). As the unit cell contains eight WO_4 ions, the correlation/Davydov splitting of internal modes leads to additional modes. Table 1 shows the correlation between irreducible representations of free ions, site group and the crystal point group. The T_d point group of the free WO_4 ion permits four different types (symmetry/irreducible representation) of vibration: A (non-degenerate), E (doubly degenerate) and F_1 and F_2 (both triply degenerate). On the other hand, crystal point group T allows only A, E and F type modes. The four internal modes ν_1–ν_4 of WO_4 have different frequencies, and undergo splitting when the ion occupies a site of lower symmetry such as C_3, e.g., $F_2 \rightarrow A + E$ [26]. The correspondence between the modes of a free ion and those of the crystal are obtained from the correlation table. Group theory predicts six modes in ν_2 region (2E + 4F), ten in the ν_4 region (2A + 2E + 6F), ten in the

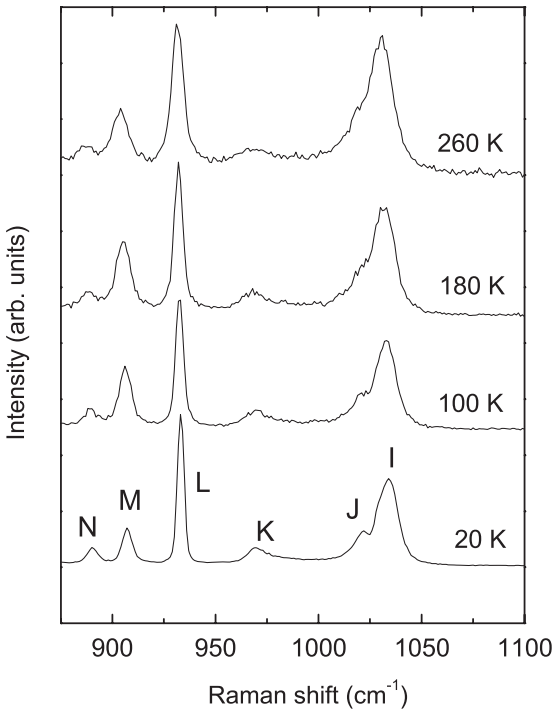

Figure 1. Raman spectra (unpolarized) of zirconium tungstate in the ν_1 mode region at different temperatures.

ν_3 region (2A + 2E + 6F) and four in the ν_1 region (2A + 2F). In contrast to expectations, the Raman spectrum at 20 K, reported earlier [11] consisted of 14 modes in the ν_3 region and six modes in the ν_1 region. The occurrence of a smaller number of modes than expected can happen due to accidental degeneracy and/or due to insufficient intensity. On the other hand, the appearance of a larger number of modes than predicted by group theory is unusual and requires a more careful examination of spectra for possible explanations. Earlier, longitudinal-optic–transverse-optic (LO–TO) mode splitting and overtones/combinations were tentatively mentioned as the cause of this [11]. This was because polarized Raman measurements had not been carried out. One can rule out the LO–TO splitting to be the cause of splitting in the ν_1 mode region of the spectrum based on the reported negligibly small infrared (IR) absorption in this region [1]. Only strong IR bands with large oscillator strength are known to cause significant LO–TO splitting. As this compound does not exhibit any modes between 433 and 628 cm^{-1}, the possibility of overtones being responsible for the peaks in the ν_1 region is also ruled out. Furthermore, overtones and combinations of different modes are expected to show different polarization characteristics; on the other hand, all the modes in the ν_1 region are found to have nearly identical polarization behaviour.

Figure 1 shows the Raman spectra of zirconium tungstate at different temperatures in the region of the ν_1 internal mode of the tungstate ion. Note that there are six peaks in the spectra labelled I to N in order of decreasing frequency. In order to assign these to the expected modes of symmetry 2A + 2F (irreducible representations), we need to analyse the A and F modes arising from correlation splitting in more detail. It is important to point out that all eight WO_4 tetrahedra in the unit cell are not identical. As mentioned earlier, there are two

Table 2. Bond lengths and bond angles for WO_4 tetrahedra and ZrO_6 octahedra using the atom positions from Evans *et al* [1].

Bond length/angle	Å/deg
W1–O4	1.724
W1–O1	1.801
W1–O (ave.)	1.782
O4–W1–O1	101.7°
W2–O3	1.694
W2–O2	1.771
W2–O (ave.)	1.752
O3–W2–O2	109.4°
W1–O3	2.430 (non-bonding)
Zr–O1	2.0395
Zr–O2	2.1168
Zr–O4	3.676 (non-bonding)
Zr–W2	6.337 (non-bonding)

distinct sets of four tungstate tetrahedra [1]. The tetrahedron around W1 is labelled as T1 and the other tetrahedron (around W2) as T2. One can see from table 2 that the bond lengths and bond angles in the two tetrahedra are quite different. From this one expects the internal mode frequencies of the two tetrahedra also to be different. Thus it is appropriate to further divide the $\nu_1(2A + 2F)$ modes into two distinct subgroups: one set of $\nu_1(A + F)$ modes belonging to four T1 tetrahedra and another set of $\nu_1(A + F)$ modes to four T2 tetrahedra. The symmetric stretching mode frequency in tetrahedral ions such as sulfates, tungstates and molybdates is known to be inversely correlated to the average bond length [27, 28]. As the average W–O bond length in the T2 tetrahedron is shorter than that in the T1 tetrahedron, the symmetric stretching mode frequency for a T2 tetrahedron is expected to be higher than that for a T1 tetrahedron. The symmetric stretching mode ν_1 is non-degenerate. As there are two distinct sets containing four WO_4 tetrahedra each, the four degrees of freedom corresponding to the ν_1 mode of $W(1)O_4$ result in vibrations A and F in the unit cell. The A mode corresponds to in-phase stretching vibration of all the four tetrahedra whereas the F mode corresponds to out-of-phase stretching vibrations where one tetrahedron expands while the other three contract. Such combinations of in-phase and out-of-phase stretching vibrations of multi-tetrahedral ions in a unit cell are known to have the same frequency [16, 29], i.e., A and F modes are degenerate. Furthermore, the four tetrahedra of the same type are well separated from each other and hence each is not expected to influence the frequency of the other three. The value of the depolarization ratio found in the present experiments also suggests the same, as described below. Similarly the other four $W(2)O_4$ tetrahedra also result in A and F degenerate modes, but at a frequency different from that of $W(1)O_4$.

One can distinguish between A and F modes from polarized measurements. For a cubic crystal the polarizability tensor for the A mode is diagonal, with identical elements. On the other hand, those for the triply degenerate F mode have only off-diagonal elements. Hence mode A will be completely polarized while that belonging to F symmetry will be completely depolarized [26]. In order to ascertain the symmetry of the ν_1 modes polarized Raman measurements were carried out on single-crystal pieces as well as on polycrystalline powder. Figure 2 shows the Raman spectra in the VV and VH polarized configurations. 'V' stands for vertical polarization and 'H' for horizontal polarization with respect to the scattering plane. The first letter corresponds to the incident polarization whereas the second to that of the analyser

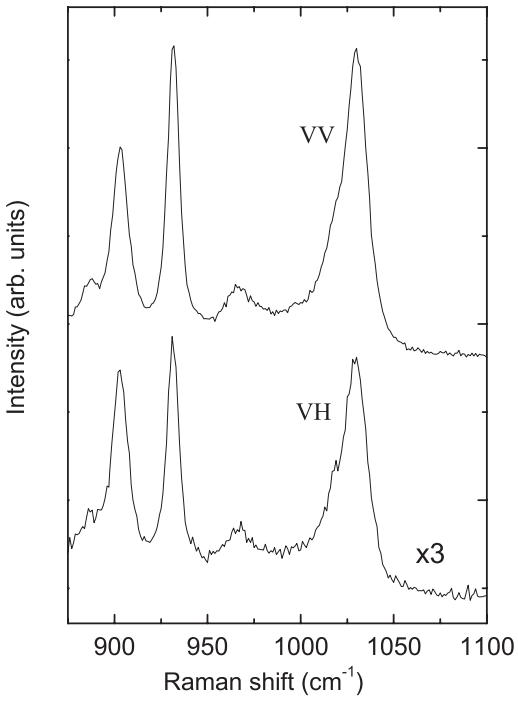

Figure 2. Polarized Raman spectra of zirconium tungstate at ambient temperature.

in the scattered light. Thus VV corresponds to polarized configuration and VH to depolarized configuration. In both cases the depolarization ratio was found to range between 0.9 and 1.1 for all six modes. This can happen only when the Raman peaks have contributions both from A and F modes, i.e., the A and F modes are degenerate. As mentioned earlier, this is also expected from symmetry considerations.

Thus from the polarized Raman measurements and symmetry arguments one expects just two modes in the ν_1 region, one each belonging to T1 and T2 tetrahedra. On the other hand, six Raman peaks are found with different relative intensities. As mentioned earlier, the appearance of a larger number of internal modes than predicted by group theory can be understood if one invokes the existence of misoriented configurations of the polyatomic ion, i.e., if some fraction of the tetrahedra are misoriented with respect to crystallographically permitted orientation/configuration at random sites. For example, a dynamic disorder of sulfate ions has been reported in potash alum [29, 30]. In the misoriented configuration the bond lengths get slightly altered leading to a new mode frequency (disorder peak) of the symmetric stretching mode. In view of this it is important to identify the two main peaks corresponding to the perfect orientations T1 and T2, and the disorder peaks. In addition, the appearance of four disorder peaks also needs to be understood. It may be pointed out that if the population of such a misoriented ion changes with temperature or pressure, the intensity of the disorder peak relative to the main peak also changes.

In order to identify the main and the disorder peaks the Raman spectra at different temperatures were quantitatively analysed and peak positions, line widths and intensities (area under the curve) obtained. Fractional intensities of different components were estimated after normalization with respect to the sum of intensities of all the six components. Figure 3 shows the temperature dependence of line widths of all the six components. Note that the most intense

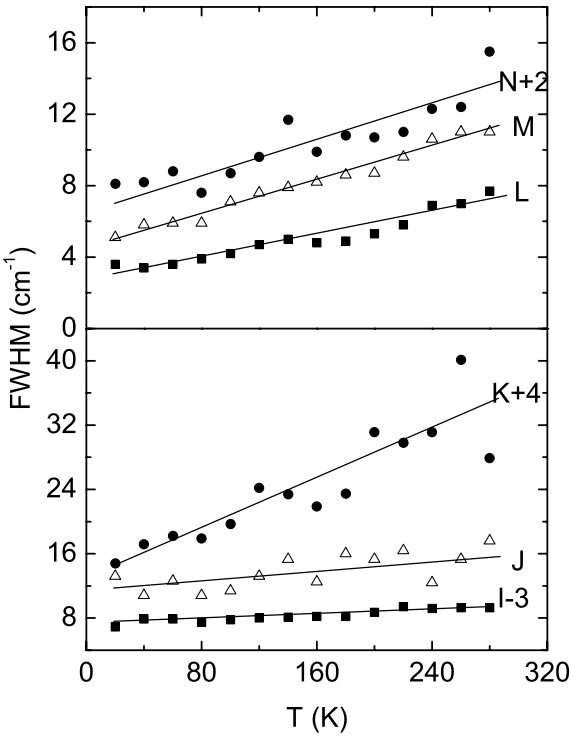

Figure 3. Temperature dependence of line widths of different components of the ν_1 mode of tungstate ions. The data for modes I, K, and N are vertically displaced for the sake of clarity.

components I and L are also the narrowest, and the line widths show the smallest slopes. In view of this it is reasonable to assign the peaks I and L to the ordered configurations of T2 and T1 respectively, and the remaining peaks to misoriented configurations. As one can see from table 2 that the bond lengths of T2 tetrahedra are smaller than those of T1 tetrahedra, the tetrahedral volume of T2 turns out to be about 3% smaller than that of T1. Hence the more compact tetrahedral ion T2 is expected to have higher ν_1 mode frequency than that of the T1 ion. Thus the component I with the highest mode frequency (1030 cm^{-1}) should be assigned to T2 and component L (931 cm^{-1}) to the T1 ion. As the tetrahedra T1 and T2 are distinct, it is reasonable to expect that misoriented configurations of T1 and T2 would result in distinct Raman peaks. However, four additional peaks are found. This suggests that the misoriented configuration of T1 also influences the vibrational frequencies of T2 in addition to that of T1 itself, and vice versa. This is possible because T1 and T2 are placed adjacent to each other in the unit cell. Another important feature of the tungstate tetrahedra is that these are not regular, and hence they are expected to have net dipole moments associated with each of the ions T2 and T1, their magnitudes **D1** and **D2** also possibly being different. From the three-fold symmetry of the two tetrahedral ions one can show that the dipoles **D1** and **D2** are aligned along the body diagonal. Figure 4 shows the oriented dipole pairs in the perfect/ideal unit cell. The magnitudes of the dipole moments are evaluated in the next section.

In order to consider various possible misoriented configurations of WO_4 ions in the unit cell, we show in figure 5(a) the arrangement of oxygen atoms around the two W atoms and the Zr atoms along the body diagonal. For the ordered configurations the dipoles are aligned

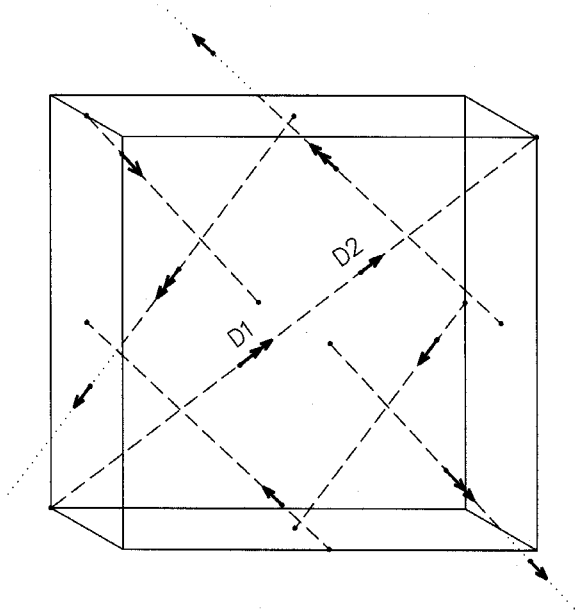

Figure 4. Cubic unit cell of $Zr(WO_4)_2$ showing oriented dipole pairs arising from distorted $WO_4(1)$ and $WO_4(2)$ tetrahedra aligned along the C_3 axis. The dipoles D1 and D2 have different magnitudes. Due to the presence of a screw axis only one dipole pair lies on the body diagonal. The D2 dipoles of the other three pairs are also shown after extending them to translationally equivalent positions in the neighbouring cells.

parallel to ⟨111⟩ directions (figure 5(b)). Note that the direction of the dipole moment vector is opposite to the W–O (terminal) bond. One can see from table 2 that the ZrO_6 octahedra are also not regular. Three Zr–O1 distances are shorter than other three Zr–O2 distances. It may be pointed out that recent time-differential perturbed angular correlation (TDPAC) experiments on partially Hf-substituted $Zr(WO_4)_2$ have shown the existence of three distinct sites for Zr(Hf) with different quadrupolar splittings [31], although one expects only a single unique site for Zr for the ideal $P2_13$ structure. Occurrence of a larger number of sites for Zr than expected for the ideal structure is consistent with the present interpretation of Raman spectra in terms of the existence of orientational disorder of tungstate tetrahedra. Misoriented configurations of T1 and T2 can result in distortion of the local environment around neighbouring Zr ions leading to two additional Zr sites.

The simplest disorder one can consider is the flipping (reversal) of terminal oxygen bond of (a) both T1 and T2 tetrahedra on the three-fold axis (figure 5(c)), (b) only T1 tetrahedron (figure 5(d)), and (c) only T2 tetrahedron (figure 5(e)). Consider first the reversal of both tetrahedra. This type of disorder indeed occurs in the β-$Zr(WO_4)_2$ (space group $Pa\bar{3}$) phase above 428 K, resulting in the symmetrization of Zr–O bond distances. Often premonitory effects of a phase transition are found near the transition temperature. In view of this it is likely that in some of the cells reversed T1–T2 pairs exist near and above 300 K, but such a reversed pair will not be distorted and will have the same site symmetry and vibrational frequency. This is because a reversed pair is equivalent to the original pair if one looks along a negative ⟨111⟩ direction (C_3 axis) (see figures 5(a) and (c)). Thus such a disorder would continue to have only single Zr site, inconsistent with the findings of TDPAC experiments. Hence this kind of disorder can be ruled out to be the cause of additional modes. On the other

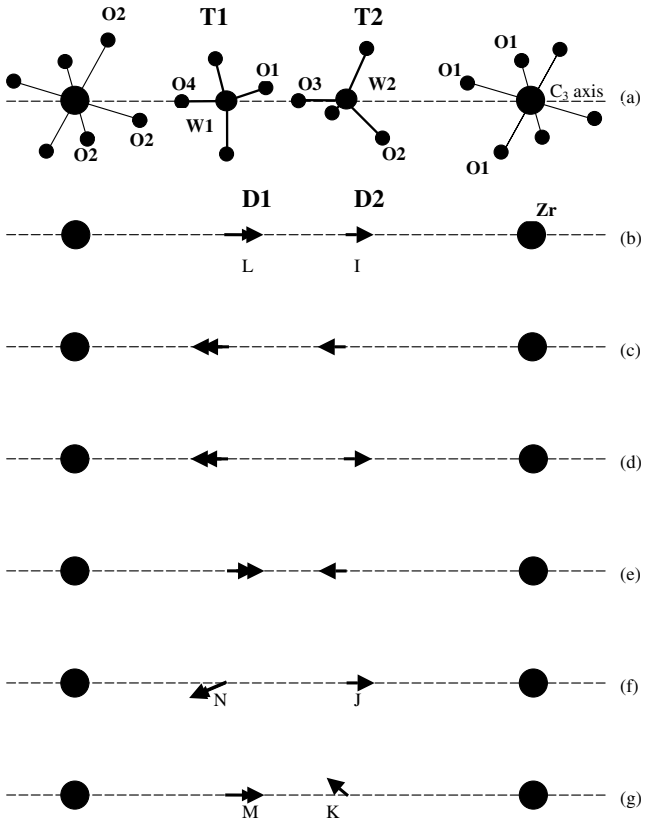

Figure 5. (a) Real-space arrangement of Zr, W1 and W2 atoms along with neighbouring O2 and O1 atoms and axial O4 and O3 atoms along the $\langle 111 \rangle C_3$ axes. (b) Orientation of dipoles **D1** and **D2** in the ordered structure. (c) Orientations of dipoles when both T1 and T2 tetrahedra are flipped (reversed). (d) Only T1 reversed. (e) Only T2 reversed. (f) Orientation of **D1** when T1 is misoriented. (g) Orientation of **D2** when T2 is misoriented. The peaks I to N of ν_1 mode of WO_4 tetrahedra are also assigned to the ordered/misoriented configurations.

hand, if T1 alone undergoes reversal, then the oxygens O3 and O4 (figures 5(a) and (d)) will come too close (almost head-on) and steric hindrance will make this configuration energetically unfavourable. We can thus rule out this configuration also. The third possibility is that of flipping of T2 tetrahedron such that both the tetrahedra point away from each other (figure 5(e)). This will cause a significant change in the vibrational frequencies due to the changes in local environment. This will also cause large displacement of W2 along the body diagonal similar to that found for the high-temperature β-phase (see figure 8 of [1]). Such displacements should manifest themselves in the diffraction experiments if the fraction of such misorientation is high. However, this misoriented configuration will keep the Zr–O bond lengths symmetric, not leading to a modified/distinct Zr site inconsistent with the TDPAC results. Thus none of the flipped configurations are likely to represent the actual orientational disorder.

We now consider a misoriented configuration of the T1 tetrahedron where the W1–O4 bond is exchanged with one of three W1–O1 bonds. Treating WO_4 as a nearly rigid tetrahedron, which has been confirmed from XAFS studies [32], one can see that such a misorientation will make the dipole **D1** point antiparallel to new W1–O4 direction (figure 5(f)), and this will also

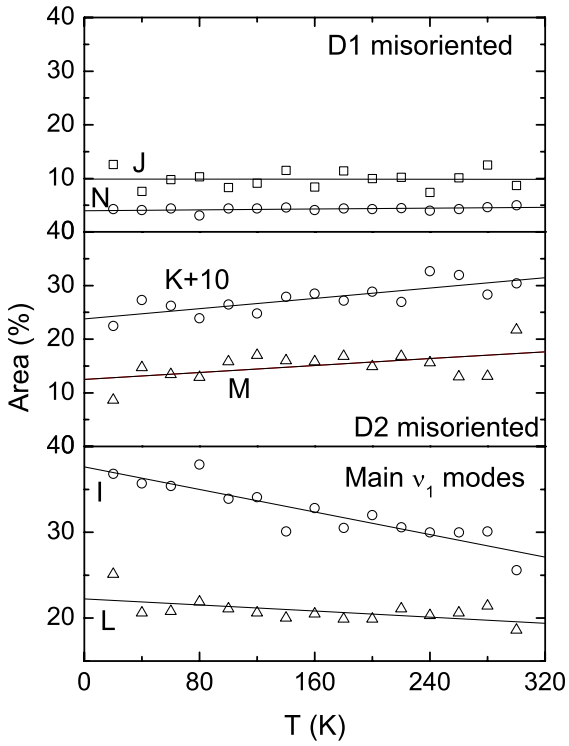

Figure 6. Temperature dependence of fractional intensities of different components of the ν_1 mode of tungstate ions in zirconium tungstate. The ordinate for the component K is displaced by $+10\%$ for the sake of clarity. The straight lines are the linear least-square fits to the data.

disturb the arrangement of oxygens around the Zr atom. In this configuration one expects the frequency of T1 to exhibit a large change whereas that of T2 to change by a smaller amount. It is also important to point out that a misoriented configuration is expected to relax its own W and O positions as well as cause relaxation of atoms in the immediate neighbourhood. Nonetheless, relaxation of the face-centre Zr atom that was bonded to O1 is also expected to occur. As the other two O1 atoms remain unaltered, the relaxation of W1 is expected to be small. This misoriented configuration indeed corresponds to a higher-energy state. This orientational disorder can either be static or dynamic. A dynamic disorder will result in the relative defect concentration to be strongly temperature dependent, obeying an Arrhenius-type relation [16]. On the other hand, if the barrier to reorientation is high, the disorder would remain static (frozen-in). In view of the much weaker T-dependence of the relative Raman intensities (figure 6) the disorder appears to be of frozen-in type. This disorder can arise during the quenching of the sample, essential for trapping of the metastable cubic phase, after synthesis at 1400 K.

The equivalent misoriented configuration of the T2 tetrahedron would correspond to a W2–O3 bond exchanged with one of the three W2–O2 bonds. This will misorient dipole **D2** antiparallel to new W2–O3 direction (figure 5(g)) and also modify the arrangement of oxygen O1 around the Zr atom. For the misoriented T2 tetrahedron the change in its frequency will be large, while the frequency of T1 will undergo a small change. Thus misoriented T1/T2 tetrahedra can each produce two additional disorder peaks in the ν_1 Raman spectra, accounting for all six peaks in this region. Furthermore, these misorientations are also expected to modify

Table 3. Symmetric stretching mode frequencies of WO_4 tetrahedra in zirconium tungstate at ambient temperature, and their assignments.

Mode label	Frequency (cm^{-1})	Assignment
I	1030	T2 (both aligned)
J	1019	T2 (T1 misoriented)
K	965	T2 (T2 misoriented)
L	931	T1 (both aligned)
M	903	T1 (T2 misoriented)
N	887	T1 (T1 misoriented)

the local oxygen environment around Zr atoms in different manners, leading to two additional Zr sites, consistent with the TDPAC results. It must be pointed out that the misorientations considered here are not taken into account in the structure refinement since the calculated and fitted intensities are for a perfect periodic lattice. The misoriented tetrahedra T1 and T2 are randomly located in some of the unit cells. For this compound the isotropic atomic displacement parameters ($U^{1/2}$) obtained from profile fitting range between 0.1 and 0.2 Å for various atoms [1]. A large part of this is possibly athermal in nature and arises due to this type of orientational disorder.

In order to elucidate the correspondence of the disorder peaks J, K, M and N with the misorientations of T1 and T2 tetrahedra we analyse the fractional intensities of all the components as a function of temperature, shown in figure 6. Among the main peaks the intensity of peak I (assigned to T2) reduces much more rapidly than that of peak L (T1). Note that out of the four disorder peaks, K and M show an increase of intensity as a function of temperature while the other two peaks, J and N, are almost temperature independent. This suggests that the populations of different misoriented configurations change with temperature in different manners. If one correlates the decrease in the intensity of main peak I (T2) with the increase in the intensities of peaks K and M, one can assign these disorder peaks to those arising from a misoriented configuration of T2 tetrahedra. The component M whose frequency (903 cm^{-1}) is close to the main component L (T1) should be assigned to T1 (**D1**$''$) while the component K (965 cm^{-1}) which exhibits a large change in frequency compared to the main component I (T2) should correspond to misoriented T2 (**D2**$'$). The other two disorder peaks J and N should then correspond to those arising from misoriented configurations of T1. In analogy with the earlier assignment, the mode J (1019 cm^{-1}) with frequency close to T2 main component I should correspond to T2 (**D2**$''$) and the component N (887 cm^{-1}), exhibiting a large change in frequency with respect to T1 main component L, can be attributed to misoriented T1 (**D1**$'$). Table 3 gives the assignment of all six components observed in the Raman spectra.

Normalized intensities of the various ν_1 lines can be analysed to obtain the fractional occupancies of ideal and misoriented configurations. It is not straightforward to calculate the scattering efficiency, and consequently the mode intensities of the normally oriented (crystallographically allowed) and the misoriented configurations of T1 and T2 tetrahedra. In the absence of any such calculations, we assume that the distorted configurations have the same scattering efficiency. Taking the intensities of the Raman peaks to be proportional to the relative populations of the tetrahedra in different configurations, the average fractional populations for perfect orientation, T1- and T2-misoriented configurations turn out to be 61 ± 4, 15 ± 2 and $24 \pm 4\%$ respectively. As a large fraction of tungstate ions are misoriented, one would expect this to be manifest in diffraction experiments. The present real-space model of disorder is

expected to cause an uncertainty in the terminal oxygen position by an amount smaller than 0.08 Å, which is consistent with atomic displacement parameters [1] of oxygen atoms obtained from profile fitting of the diffraction intensities. An alternative way to understand this disorder would be that the material actually has lower symmetry than $P2_13$ and results in an average cubic symmetry due to micro-twinning. It is also likely that the scattering efficiency of different orientations of T1 and T2 could be different. If the disordered sites had higher efficiency then a smaller concentration of defects could also yield the same Raman intensity. From the intensities of the components the temperature dependence of the populations of misoriented T1 and T2 tetrahedra appear to be different. The misoriented T1 tetrahedra population shows some increase as a function of temperature, while that of T2 shows much weaker temperature dependence. The difference in the behaviour of the two tungstate ions may arise due to the difference in the activation barrier for reorientation.

It is important to point out that the misoriented configurations of T1 and T2 visualized here correspond to simple reorientations of the tetrahedra. It is likely that the actual misoriented configurations may be relaxed and become more complex in nature. In order to confirm whether the proposed misoriented configurations are energetically stable or not, we have carried out density-functional calculations using the SIESTA code [23]. We have examined the stability of the tetrahedral WO_4 ions in the ideal defect-free structure and also after flipping one of the long W–O bonds with the short W–O bond along the body diagonal. This is equivalent to a rotation of the tetrahedron about an axis centred on the W atom, such that the short bond is interchanged with one of the long bonds, without any distortion in the tetrahedron. Starting from the unrelaxed ideal structure three different calculations have been carried out: (i) $Zr(WO_4)_2$ crystal in the defect-free ideal structure, and in two different defect structures generated by (ii) a rotation of the tetrahedron centred on the W1 atom and (iii) a rotation of the tetrahedron centred on the W2 atom. First, all the atom positions in the ideal structure were relaxed to find the minimum energy configuration and the equilibrium lattice parameter. This relaxed structure was used as the reference against which the stabilities of the defect structures were examined. All the atoms in the defect structures were relaxed with no constraints on the structure until the interatomic forces became smaller than 5 meV $Å^{-1}$.

The lattice parameter of the relaxed ideal structure was found to be 9.4814 Å, about 3.26% higher than the reported value at 0.3 K. Similar to the relaxed ideal structure, all the defect configurations also preserve the cubic unit cell structure. Table 4 summarizes the results of the calculations, giving the defect energies and the bond distances for the defect configurations and for the defect-free ideal lattice along with those obtained from Rietveld refinement of the diffraction data. The defect structure, in which the T2 tetrahedron is rotated, is higher in energy as compared to that with the rotated T1 tetrahedron. The difference arises due to the different local environment of the T1 and T2 tetrahedra. As the energies required to create these defects are high, these are not the equilibrium defects at ambient temperature. However, as pointed out earlier, these can be created during quenching of the sample subsequent to synthesis at ∼1400 K. After relaxation, the bond distances in both the tetrahedra are found to change. The short bond gets elongated slightly whereas the long bond gets shortened; however, the bonds do not relax to the original lengths. One can also note that T1 tetrahedron rotation causes the neighbouring T2 bonds also to relax and vice versa, consistent with the proposed model. The bond angles are also found to change by a few degrees, suggesting distortions of the tetrahedra. These changes in the bond lengths for the defect configurations will result in additional frequencies of the internal vibrations of the tetrahedra consistent with the present interpretation of the Raman spectra. To summarize, the density-functional calculations indeed confirm that the proposed defect configurations are energetically stable and lead to new bond distances that can result in additional modes.

Table 4. Relaxed W–O bond distances and defect energies obtained from density-functional calculations using the SIESTA code starting from the ideal defect-free (unrelaxed) Rietveld refined structure.

	Ideal structure		T1	T2
	Diffraction-unrelaxed	SIESTA-relaxed	tetrahedron rotation	tetrahedron rotation
ΔE (eV)	+31.04	0.00	+3.38	+7.09
Bond distances (Å)				
W1–O4	1.724	1.774	1.831	1.773
W1–O1	1.801	1.844	1.834	1.803
W1–O1	1.801	1.844	1.879	1.805
W1–O1	1.801	1.844	1.884	1.793
W2—O3	1.694	1.808	1.797	1.835
W2–O2	1.771	1.876	1.862	1.816
W2–O2	1.771	1.876	1.860	1.851
W2–O2	1.771	1.876	1.865	1.837

As mentioned earlier, the non-regular nature of the two tetrahedra results in net dipole moments aligned along the body diagonals. It is important to obtain their magnitudes and discuss the consequences of the orientational disorder. In order to calculate the dipole moments one requires the atom positions and charges on them. The simplest model is to take the charges to be +6 and −2, corresponding to fully ionized W and O atoms respectively (the full-charge model). However, different effective charges have been chosen in the earlier theoretical studies of phonon dispersion [33] and electronic structure [34]. As different initial input parameters of effective charge yield satisfactory vibrational and electronic properties, we have used both these charge parameters as well as those of the full-charge model. As the site symmetry of the two tungstate tetrahedra is C_3, the centre of positive and all negative charges lies on the three-fold axis. For the purpose of calculation of the dipole moment the net charge on the tetrahedra is assumed to be uniformly distributed only among the three non-terminal oxygens (O1 or O2). As a first approximation this is reasonable because the terminal oxygens (O3 and O4) do not bond to the Zr atoms. Table 5 gives the input charge parameters and the calculated dipole moments for all three models. The important thing that emerges from this calculation is the large difference in the magnitudes of **D1** and **D2**. Although one expected the magnitudes of the dipole moments to be different from qualitative arguments, the extent of difference could be found only from this calculation. These pairs of dipoles between two Zr atoms essentially form four separate chains running along the four body diagonals; however, these chains are displaced with respect to each other due to the presence of the screw axis, and do not intersect each other. The net dipole moment in the unit cell is zero for the ideal lattice (perfect aligned configuration). However, orientational disorder of T1 and T2 can result in randomly misoriented dipoles in different unit cells. These are essentially frozen-in misoriented dipoles. From this it appears that these misoriented dipoles could create a dipole-glass state. Dipole-glasses were first reported in alkali halides doped with molecular ions with permanent dipole moments such as OH^-, CN^- and NH_4^+ [35–38]. Freezing of randomly oriented dipole moments in different unit cells led to dipole-glass behaviour. Dipole-glass has also been found to form in doped ferroelectric materials such as $KTaO_3$:Li, $SrTiO_3$:Ca, and other compounds [39, 40]. In these systems the dipole-glass is believed to arise due to freezing of superparaelectric clusters [41]. All these systems are invariably doped or mixed-crystal systems. Zirconium tungstate is possibly the first example of an intrinsic dipole-glass

Table 5. Effective charges (in units of *e*) on various atoms based on three different model input parameters and the calculated dipole moments on tungstate ions.

	Full charge model	Chaplot (1999)	Oyang (2003)
Zr	+4	+2.2	+2.65
W1	+6	+3.3	+5.27
W2	+6	+3.3	+5.22
O1	−2	−1.1	−1.61
O2	−2	−1.1	−1.61
O3	−2	−1.1	−1.72
O4	−2	−1.1	−1.75
Net charge on T1	−2	−1.1	−1.31
Net charge on T2	−2	−1.1	−1.33
D1 (Debye)	9.50	5.23	8.31
D2 (Debye)	4.97	2.73	4.10

arising from the orientational disorder of tungstate ions. Recently the thermal conductivity of zirconium tungstate has been found to be low, glass-like, and close to its theoretical minimum value based on fully coupled phonons [22]. Misoriented tungstate ions are expected to be efficient scattering centres for phonons, leading to poor thermal conduction. Thus the existence of glass-like thermal conductivity even in the crystalline state appears to be consistent with the presence of orientational disorder. It is worth comparing the magnitude of the dipole moment on the tungstate ion with that of a water molecule, which results in unique dielectric properties of liquid water. The water molecule has a dipole moment of ∼2 Debye [42], which is only about one fifth of that of the tungstate tetrahedron T1. This suggests that the dipolar interactions in zirconium tungstate are likely to result in very interesting dielectric behaviour.

5. Summary and conclusions

To summarize, a detailed analysis of the number of vibrational Raman peaks in the ν_1 symmetric stretching mode region and their temperature dependences suggest the existence of disorder in the orientations of tungstate tetrahedra. The components of the ν_1 Raman spectra could be assigned to two ordered peaks and four disorder peaks. Different disordered configurations are visualized as there exist distinct WO_4 tetrahedra. First-principles density-functional calculations confirm the stability of the proposed misoriented WO_4 configurations. The misorientations considered here change the directions of the dipole moment associated with the tungstate ions in the lattice. The magnitudes of the dipole moments are found to be much more than that of a water molecule. The glass-like thermal conductivity reported in this system may have its origin in the randomly misoriented dipoles leading to a possible dipole-glass state.

Acknowledgments

We thank an anonymous referee for many useful remarks. We acknowledge Dr T A Mary for the samples, Dr R Govindaraj for discussing perturbed angular correlation results prior to publication, and Mr M C Valsakumar for stimulating discussions. We also thank Dr C S Sundar for interest in the work, Dr P R Vasudava Rao for support and Dr Baldev Raj for encouragement.

References

[1] Evans J S O, Mary T A, Vogt T, Subramanian M A and Sleight A W 1996 *Chem. Mater.* **8** 2809
[2] Ravindran T R, Arora A K and Mary T A 2000 *Phys. Rev. Lett.* **84** 3879
[3] Cao D, Bridges F, Kowach G R and Ramirez A P 2003 *Phys. Rev.* B **68** 014303
[4] Mittal R, Chaplot S L, Kolesnikov A I, Loong C K and Mary T A 2003 *Phys. Rev.* B **68** 054302
[5] Ravindran T R, Arora A K and Mary T A 2003 *Phys. Rev.* B **67** 064301
[6] Hancock J N, Turpen C, Schlesinger Z, Kowach G R and Ramirez A P 2004 *Phys. Rev. Lett.* **93** 225501
[7] Sivasubramanian V, Ravindran T R, Nithya R and Arora A K 2004 *J. Appl. Phys.* **96** 387
[8] Ravindran T R, Sivasubramanian V and Arora A K 2005 *J. Phys.: Condens. Matter* **17** 277
[9] Evans J S O, Mary T A and Sleight A W 1997 *J. Solid State Chem.* **133** 580
[10] Evans J S O and Mary T A 2000 *Int. J. Inorg. Mater.* **2** 143
[11] Ravindran T R, Arora A K and Mary T A 2001 *J. Phys.: Condens. Matter* **13** 11573
[12] Hanuza J and Macalik L 1987 *Spectrochim. Acta* A **43** 361
[13] Yamamura Y, Nakajima N and Tsuji T 2000 *Solid State Commun.* **114** 453
[14] Jorgensen J D, Hu Z, Teslic S, Argyriou D N, Short S, Evans J S O and Sleight A W 1999 *Phys. Rev.* B **59** 215
[15] Arora A K, Nithya R, Yagi T, Miyajima N and Mary T A 2004 *Solid State Commun.* **129** 9
[16] Sood A K, Arora A K, Dattagupta S and Venkataraman G 1981 *J. Phys. C: Solid State Phys.* **14** 5215
[17] Arora A K and Sakuntala T 1992 *J. Phys.: Condens. Matter* **4** 8697
[18] Sakuntala T, Arora A K, Shekar N V C and Sahu P Ch 1998 *Europhys. Lett.* **44** 728
[19] Sakuntala T, Arora A K, Shekar N V C and Sahu P Ch 2000 *J. Phys.: Condens. Matter* **12** 4417
[20] Guthoff F, Ohl M, Reehuis M and Loidl A 1999 *Physica* B **266** 310
[21] Velardez G F, Alavi S and Thompson D L 2004 *J. Chem. Phys.* **120** 9151
[22] Kennedy C A and White M A 2005 *Solid State Commun.* **134** 271
[23] Soler J M, Artacho E, Gale J D, Garcia A, Junquera J, Ordejon P and Portal D S 2002 *J. Phys.: Condens. Matter* **14** 2745
[24] Scott J F 1968 *J. Chem. Phys.* **48** 874
[25] Baisev T T, Sobol A A, Voronko Yu K and Zverev P G 2000 *Opt. Mater.* **15** 205
[26] Turrel G 1972 *Infrared and Raman Spectra of Crystals* (New York: Academic)
[27] Arora A K 1997 *Adv. High Pressure Sci. Technol.* ed M Yousuf, N Subramanian and K G Rajan (Hyderabad: Universities Press) p 162
[28] Daniel M F, Desbat B, Lassegues J C, Gerand B and Figlarz M 1987 *J. Solid State Chem.* **67** 235
[29] Eysel H H and Schumacher G 1977 *Chem. Phys. Lett.* **47** 168
[30] Larson A C and Cromer D T 1967 *Acta Crystallogr.* **22** 793
[31] Govindaraj R 2006 private communication
[32] Cao D, Bridges F, Kowach G R and Ramirez A P 2002 *Phys. Rev. Lett.* **89** 215902
[33] Mittal R and Chaplot S L 1999 *Phys. Rev.* B **60** 7234
[34] Ouyang L, Xu Y-N and Ching W Y 2002 *Phys. Rev.* B **65** 113110
[35] Paul M S, Mesa M and Nava R 1983 *Solid State Commun.* **47** 183
[36] Wang C H and Satija S K 1982 *Chem. Phys. Lett.* **87** 330
[37] Yagi K, Sakaue K and Terauchi H 2001 *J. Synchotron Radiat.* **8** 806
[38] Vugmeister B E and Glinchuk M D 1990 *Rev. Mod. Phys.* **62** 993
[39] Prosandeev S A, Trepakov V A, Savinov M E, Jastrabik L and Kapphan S E 2001 *J. Phys.: Condens. Matter* **13** 9749
[40] Ranjan R and Pandey D 2001 *J. Phys.: Condens. Matter* **13** 4239
[41] Shabbir G, Ko J-H and Kojima S 2005 *Appl. Phys. Lett.* **86** 012908
[42] Yu H and van Gunsteren W F 2004 *J. Chem. Phys.* **121** 9549